The effect of Ag-doping (x = 0 and 0.05) on structural and morphological $La_{0.8-x}Ag_xCa_{0.2}MnO_3$ material synthesized by sol-gel method

IOP Conf. Series: Materials Science and Engineering **496** (2019) 012019 doi:10.1088/1757-899X/496/1/012019

The effect of Ag-doping (x = 0 and 0.05) on structural and morphological $La_{0.8-x}Ag_xCa_{0.2}MnO_3$ material synthesized by sol-gel method

R Kamila and B Kurniawan

Department of Physics, Faculty of Mathematics and Natural Sciences (FMIPA)
Universitas Indonesia, Depok 16424, Indonesia

Corresponding author: bkuru@fisika.ui.ac.id

Abstract. In this paper, we will report the Ag-doping effect on the structure and morphology of $La_{0.8}Ca_{0.2}MnO_3$ (LCMO) and $La_{0.75}Ag_{0.05}Ca_{0.2}MnO_3$ (LACMO) materials. LCMO and LACMO materials were synthesized via the sol-gel method and sintered at 900 °C for 24h. The structure of the materials was characterized using X-Ray Diffractometer (XRD) and found that both materials are in the orthorhombic structure (Pnma space group). Scanning Electron Microscopy (SEM) was used to observe the morphology of the material and obtained the homogeneity of the materials. With Ag doping, the grain size of the material will decrease. The results of Electron Dispersive Spectroscopy (EDS) confirm the composition of both materials.

1. Introduction

The perovskite manganite material which has the form $Rn_{1-x}A_xMnO_3$, with A as divalent cations from alkaline earth elements (Ca, Ba, Sr, or Pb) and Rn as trivalent cations of rare earth element (La, Nd, Cd, or Pr), has been widely studied because of its attractive properties such as physical, magnetic, or transport properties [1]. The attractive properties of this perovskite manganite provide many potential fields to be applied such as sensors, magnetic refrigeration, magnetic memory device, etc. [1]. The divalent alkaline earth cation element is doped to substitute the trivalent rare earth cation element will give variation to the valence of Mn, Mn^{3+} and Mn^{4+}. The existence of various Mn valences can produce the Double Exchange (DE) interaction phenomenon between $Mn^{3+}-Mn^{4+}$. In the DE phenomenon, for example, electrons can hop between Mn^{3+} and Mn^{4+} with oxygen as an intermediary. The strength of the DE interactions influences the magnetic and transport properties of $Rn_{1-x}A_xMnO_3$ material [2]. Doping other element to Rn, A, or Mn can cause lattice distortion and affect the DE phenomenon [3]. The inter-grain distance, such as the length of the Mn-O bond, plays a role in the transport properties of the material. Therefore, the structure and morphology of the material is important to be known.

In this paper, silver (Ag) will be doped to substitute Lanthanum (La). The structure and morphology will be observed as the results of Ag-doping. Ag doping is expected to reduce grain boundary. Ag was chosen because it can improve the electrical properties of LCMO materials [4]. Ag doping can also provide inter-granular conduction pathways [5]. It is expected that Ag doping to LCMO parents can enhance DE interactions, increase the Curie temperature, and provide a large magnetoresistance effect.

In previous studies, LCMO and LACMO materials were mostly synthesized by solid-state methods. In this paper, the materials were synthesized by the sol-gel method to obtain better homogeneity and only require low temperatures process. In addition, not many researchers conducted LCMO comparisons before and after La was substituted by Ag. Most studies doped Ag to change Ca concentrations.

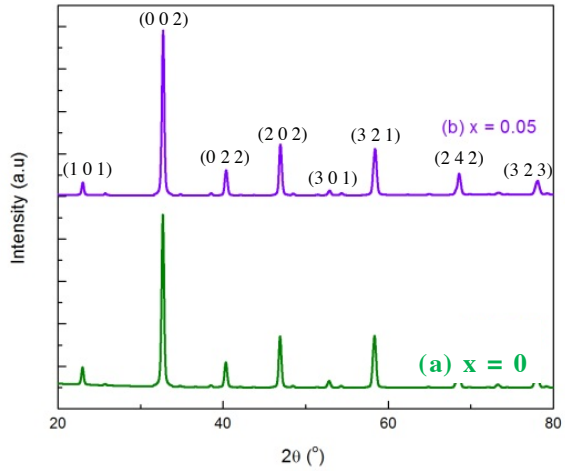

Figure 1. XRD pattern of $La_{0.8-x}Ag_xCa_{0.2}MnO_3$ (a) x = 0 and (b) x = 0.05.

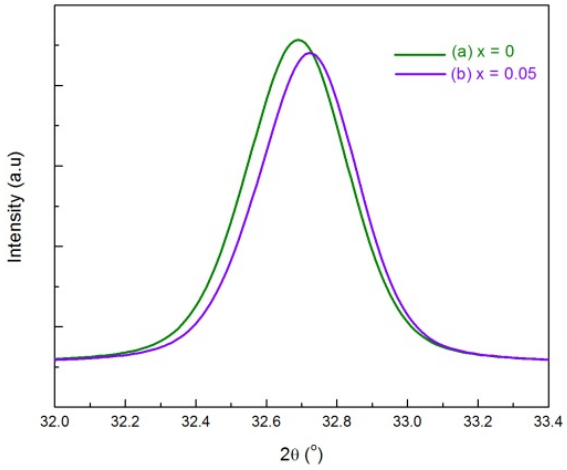

Figure 2. Local XRD patterns at the strongest peak (002) of $La_{0.8-x}Ag_xCa_{0.2}MnO_3$ (a) x = 0 and (b) x = 0.05.

2. Experimental

$La_{0.8-x}Ag_xCa_{0.2}MnO_3$ (x = 0 and 0.05) were prepared by the sol-gel method. The precursors used are nitrate based such as $AgNO_3$, $Ca(NO_3)_2.6H_2O$, and $Mn(NO_3)_2.4H_2O$. La_2O_3 powder is dissolved using HNO_3 solution to become a La nitrate solution. $C_6H_8O_7.H_2O$ was used as a catalyst of the solution. The PH of the solution was adjusted until it reaches 7 by an ammonia solution. The solution was mixed and stirred using a magnetic stirrer at a preserved temperature of 80-90 °C until it is formed into a highly viscous gel. Furthermore, the samples were dehydrated at 120 °C for 3 h, calcined at 500 °C for 6 h to decompose organic compounds, and pressed into pellets. Last, samples were sintered at 900 °C for 24h to grow crystal bonds.

The structural properties of the material were characterized using XRD (Rigaku-Smartlab, 3kV) and carried out at room temperature conditions of 18-25 °C. Scanning Electron Microscope (Hitachi SU-3500) was used to observe the morphology and homogeneity of LCMO and LACMO materials. The magnification of the SEM used is 20.000x using Secondary Electron (SE) and Backscattered Electron (BSE) modes. BSE mode indicates the material homogeneity and SE mode contains material topographic information. Material composition and its purity were confirmed by Energy Dispersive X-ray Spectroscopy (EDS) Horiba. The area chosen in the EDS characterization was carried out to ensure that Ag was successfully doped to substitute La, which supported the XRD results obtained.

3. Results and discussion

3.1. Crystal structure

LCMO and LACMO structures were characterized using XRD. The XRD results of the two materials are shown in figure 1. The XRD patterns show there no additional peak other than Ag after doping with Ag. The XRD patterns also show the occurrence of a small shift in position of the highest peak (figure 2). A shift to a slightly larger angle value indicates a decrease in lattice parameters with Ag doping [4].

The structural parameters of the refinement results for LCMO and LACMO materials are summarized in table 1. The structure of both LCMO and LACMO crystals are orthorhombic with the Pnma space group no 62. The structure of the two crystals remains the same with the Ag doping. This shows that Ag doping does not change the crystal structure. After doping by Ag elements, all crystal lattice parameter show a decrease in value. This occur because of the radius of the Ag^+ ion is smaller than the radius of the La^{3+} ion, which results in a decrease in unit cell volume and other lattice parameters. The ion radii of the LCMO and LACMO materials are shown in table 2 [1,2]. Table 3 and

Table 1. Refined structural parameters of $La^{3+}_{0.8-x}Ag^{+}_{x}Ca^{2+}_{0.2}MnO_3$ (x = 0 and 0.05).

Structural parameters	x = 0	x = 0.05
Crystal structure	Orthohombic	Orthohombic
Space group	Pnma	Pnma
a (Å)	5.4696	5.4643
b (Å)	7.7361	7.7256
c (Å)	5.4969	5.4945
Volume (Å^3)	232.5991	231.9542
<Mn-O> (Å)	1.9636	1.9633
<Mn-O-Mn> (^{o})	162.185	161.149
χ^2	1.17	1.13

Table 2. Ionic radii of each ion in $La^{3+}_{0.8-x}Ag^{+}_{x}Ca^{2+}_{0.2}MnO_3$ (x = 0 and 0.05).

Ion	Radii (nm)
La^{3+}	1.36
Ag^{+}	1.28
Ca^{2+}	1.12
Mn^{3+}	0.65
Mn^{4+}	0.53
O^{2-}	1.4

Table 3. Complete crystallographic parameters of $La_{0.8}Ca_{0.2}MnO_3$ material

Atom	Atomic position			Wyckoff factor	Occu-pancy
	x	y	z		
La	0.4824	0.25	0.003	4c	0.8
Ag	-	-	-	-	-
Ca	0.4824	0.25	0.003	4c	0.2
Mn	0	0	0	4a	1
O1	0.2262	0.0327	0.2696	8d	1
O2	0.5024	0.25	0.5645	4c	1

Table 4. Complete crystallographic parameters of $La_{0.75}Ag_{0.05}Ca_{0.2}MnO_3$ material

Atom	Atomic position			Wyckoff factor	Occu-pancy
	x	y	z		
La	0.4824	0.25	0.003	4c	0.75
Ag	0.4824	0.25	0.003	4c	0.05
Ca	0.4824	0.25	0.003	4c	0.2
Mn	0	0	0	4a	1
O1	0.2262	0.0327	0.2696	8d	1
O2	0.5024	0.25	0.5645	4c	1

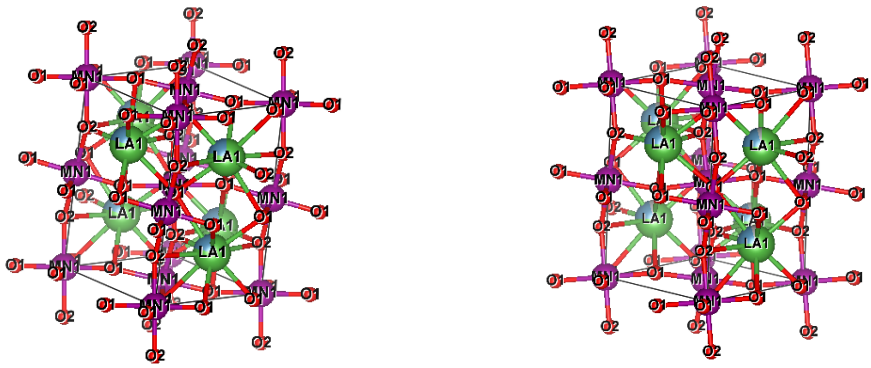

(a) (b)

Figure 3. Crystal structure of (a) $La_{0.8}Ca_{0.2}MnO_3$ and (b) $La_{0.75}Ag_{0.05}Ca_{0.2}MnO_3$ material

table 4 present complete crystallographic parameters, which consist of atomic position, Wyckoff factor, and occupancy of each atom that making up the material. The unchanging crystal structure can also be seen from the Wyckoff factor, which has not changed after being doped by Ag. The average crystallite size of LCMO and LACMO were calculated using Debye-Scherrer equation, each obtained 44.89 nm and 33.18 nm, respectively. However, changes in lattice parameters that occurred were not significant with Ag doping because of small-scale doping concentrations. This indicates a slight change in lattice parameters but does not change the crystal structure. The crystal structure of both materials is shown in figure 3.

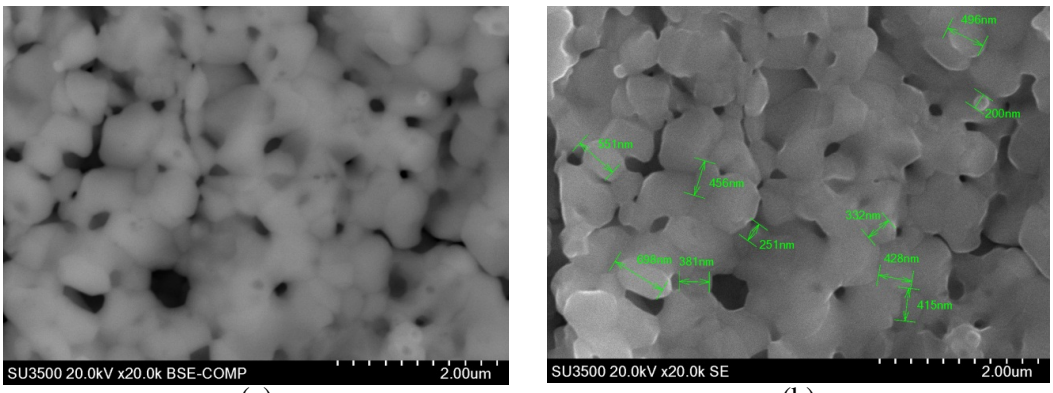

(a) (b)

Figure 4. SEM images using (a) BSE and (b) SE mode on $La_{0.8}Ca_{0.2}MnO_3$ material

The length of the Mn-O bond and the Mn-O-Mn angle were obtained using refinement analysis of the XRD pattern (table 1). The results show a decrease in the length of Mn-O bond. Changes in the length of Mn-O bond could affect the nature of material transport [3]. Winarsih *et al.* [3] explained this by using a core-shell model, which uses distance of the grain as a half value of d, which is the distance of Mn and O ions [3]. Thus, if inter-grain distance gets wider, it could weaken the DE interaction and electron transport will be more difficult, which will result in increased material. Moreover, the DE interaction is also related to conduction bandwidth (W), where $W \sim \cos(\pi - \theta_{Mn\text{-}O\text{-}Mn}) / d_{Mn\text{-}O}$ with $\theta_{Mn\text{-}O\text{-}Mn}$ as Mn-O-Mn bond angle and $d_{Mn\text{-}O}$ as Mn-O bond distance [6]. It can be seen, if the distance of Mn-O ions becomes shorter, the bandwidth conduction value will be greater and strengthen the DE interaction, which will affect the material transport properties. By doping Ag^{+} ions to substitute La^{3+} ion, it can shorten the distance of Mn-O so that it is expected to increase the nature of material transport.

Furthermore, changes in the Mn-O bond distance can be obtained from the FT-IR measurements. Based on previous research by Daengsakul *et al.* [7] who studied the functional groups presence in $LaMnO_3$ material using FT-IR that there is a stretching mode on the absorption band at wavenumber 600 cm^{-1} because of internal motion that change the Mn-O bond distance [7]. Another study conducted by Shinde *et al.* [8] for $La_{0.8}Ca_{0.2}MnO_3$ material producing the FT-IR spectra, which show similar things that the main absorption band around wavenumber 600 cm^{-1} is associated with the presence of oxygen metal bonds in the perovskite structure that involves internal motion that changes the Mn-O bond distance [8]. Based on previous researches, doping Ag to substitute La^{3+} will produce a stretching mode with a change in the Mn-O bond distance from the XRD results. However, this cannot be explained more deeply because it is only based on XRD data.

3.2. Morphology

Figure 4 and Figure 5 show SEM images of LCMO and LACMO materials. From BSE mode, LCMO and LACMO materials have good homogeneity because the colour contrast is quite uniform. From SEM observations, it can be seen that the grain of both materials have a granular shape that are in accordance with previous studies [9,10]. Next, the grain size of LCMO and LACMO materials obtained grain sizes ranging from 200–698 nm with an average grain size of 420.8 nm for LCMO and with an average grain size of 347 nm for LACMO. The presence of various grain sizes occurs due to agglomeration so that grain size measurements are not appropriate. Observation of grain size from SEM characterization is greater than the crystallite size obtained from the Debye Scherrer equation using XRD results. The results also show that each grain from SEM results consists of several crystals.

3.3. Composition and purity

The material composition of LCMO and LACMO were confirmed by EDS measurements. The results of the observation are shown in table 5. The EDS results show that the atomic fraction values from measurement are close to the calculated atomic fraction values, which indicate that LCMO and LACMO materials are succeessfully synthesized according to the desired composition. The small

Table 5. Compositional results of $La_{0.8-x}Ag_xCa_{0.2}MnO_3$ (x = 0 and 0.05).

Doping concentrations	Element (% at.)									
	La		Ag		Ca		Mn		O	
	Calc	Obs	Calc	Obs	Calc	Obs	Calc	Obs	Calc	Obs
x = 0	16	18.06	0	0	4	3.44	20	17.69	60	60.82
x = 0.05	15	13.31	1	0.4	4	3.62	20	16.54	60	66.13

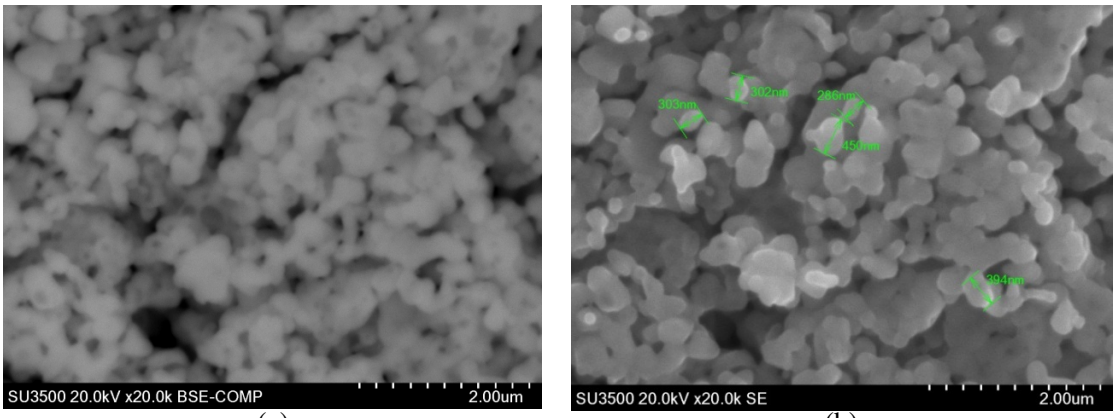

(a) (b)

Figure 5. SEM images using BSE and SE mode on $La_{0.75}Ag_{0.05}Ca_{0.2}MnO_3$ material

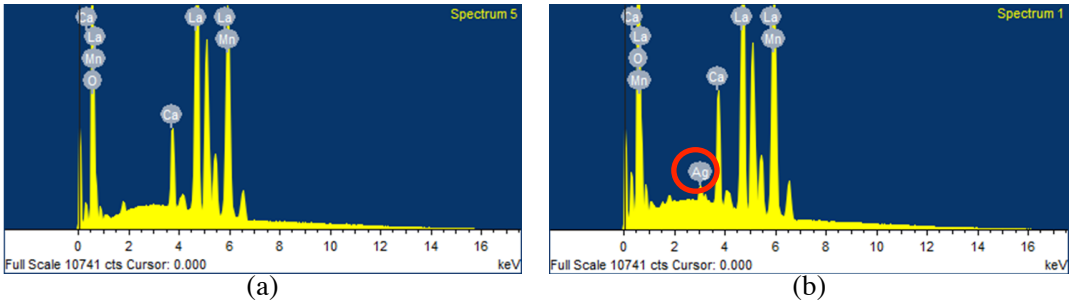

(a) (b)

Figure 6. Measurement results of EDS analysis $La_{0.8-x}Ag_xCa_{0.2}MnO_3$
(a) x = 0 and (b) x = 0.05.

difference between the atomic fraction from EDS measurement results and the results occurs because EDS provides a semi-quantitative analysis. Therefore, the results from the EDS are only close to the results of the calculation.

Furthermore, the measurement results of EDS in figure 6 shows the presence of Ag element in LACMO material. This indicates that the Ag element has successfully doped to the LCMO material and substituting La.

4. Conclusions

$La_{0.8-x}Ag_xCa_{0.2}MnO_3$ (x = 0 and 0.05) were successfully synthesized by the sol-gel method. The XRD results showed that Ag doping did not change the crystal structure of the materials and still remained the same as the orthorhombic. The lattice parameters and unit cell volume of the crystal decrease with Ag doping due to the smaller ionic radius of the Ag^+ ion than the ion radius of La^{3+}. Decreasing the length of the Mn-O bond due to Ag doping will make the DE phenomenon stronger and affect the material transport properties. Microstructure results from SEM showed that both of materials had a granular form grain with an average size of 257.17 nm for LCMO and 289.9 nm for LACMO. The

EDS results supported the XRD results and show that Ag is successfully doped into the material. The value of atomic fraction observed by EDS approaches the calculated value.

Acknowledgements
The research is funded entirely by PITTA Grant 2017 from Universitas Indonesia under contract number 633/UN2.R3.1/HKP.05.00/2017.

References
[1] Smari M, Hamouda R, Walha I, Dhahri E, Mompeán F J and Garcia-Hernández 2015 *J. Alloys Compd.* **644** 632–7
[2] Ye S L, Song W H, Dai J M, Wang K Y, Wang S G, Zhang C L, Du J J, Sun Y P and Fang J 2002 *J. Magn. Magn. Mater.* **248** 26–33
[3] Winarsih S, Kurniawan B, Manaf A, Saptari S A and Nanto D 2016 *J. Phys.: Conf. Ser.* **776** 012058
[4] Yin X P, Liu X, Yan Y Z and Chen Q M 2014 *J. Sol-Gel Sci. Technol.* **70** 361–5
[5] Huang Y H, Huang K F, Luo F, He L L, Wang Z M, Liao C S and Yang C H 2003 *J. Solid State Chem.* **174** 257–63
[6] Kurniawan B, Winarsih S, Ramadhan M R, Naomi A and Laksmi W 2017 *AIP Conf. Proc.* **1862** 030048
[7] Daengsakul S, Mongkolkachit C, Thomas C, Thomas I, Siri S, Amornkitbamrung V and Maensiri S 2009 *Optoelectron. Adv. Mater. Rapid Commun.* **3** 106–9
[8] Shinde K P, Oh S S, Baik S K, Kim H S, Sinha B B and Chung K C 2012 *J. Korean Phys. Soc.* **61** 2000–4
[9] Xi S, Lu W and Sun Y 2012 *J. Appl. Phys.* **111** 063922
[10] Kalyana L Y and Reddy P V 2010 *Solid State Sci.* **12** 1731–40